Global Journal of Computer and Engineering Technology (GJCET)

Vol. 3, No. 1, January, 2023 ISSN: 2767-1933

IDENTIFICATION OF WIND TURBINES FROM SATELLITE IMAGES USING A DEEP NEURAL NETWORK

Pushpalata Pujari, Guru Ghasidas Vishwavidyalaya, India (pujari.lata@rediffmail.com)
Himanshu Sahu, Guru Ghasidas Vishwavidyalaya, India (himanshusahu115581@gmail.com)

ABSTRACT

Identification of wind turbines has immense importance for land and resource management. The location of wind turbines provides a better understanding of issues related to radar wind and renewable energy supply. It helps in environmental impacts, change monitoring, and planning of new wind turbine locations and radar. Due to the complexities in the background, noise, size, and distance parameters automatic detection of wind turbines become a challenging issue in the present scenario. This article presents an effective methodology for the identification of wind turbines from satellite images using a Deep Neural Network (DNN). Residual Network-50(ResNet-50) has been applied to the subset of the wind turbine data consisting of 1000 satellite images taken from the Kaggle dataset. The satellite images include images of wind turbines with backgrounds and backgrounds without wind turbines. First, the satellite images are pre-processed to improve the quality of images before they are used in the training phase by suppressing undesired distortions. Performance metrics such as validation loss, accuracy, error rate, precision, recall, F1 score, and area under the curve have been used to assess the proposed model's performance. The outcomes of the proposed model are also contrasted with those of alternative ResNet architectures. According to the results of the experimental study, the proposed ResNet-50 model has outperformed other ResNet models and has obtained an accuracy of 98%. The acquired findings support the applicability of the proposed approach to the global dynamic identification of wind turbines from satellite images.

Keywords: Deep Neural Network, ResNet-50, CNN, Wind Turbines patches

1. INTRODUCTION

One of the requirements of the present world is to generate clean energy through wind turbines which can reduce the emission of carbon dioxide gas from traditional methods to a great extent. Wind turbines are the primary source of renewable energy which can produce clean and sustainable energy. From the environmental point of view, the energy produced from wind turbines is an alternative source to non-renewable energy. Identification of wind turbines has immense importance for the evaluation of installed capacity, automatic cartography, environmental surveys, and many more. A robust solution is needed for the identification of wind turbines. Wind turbines are well captured by satellite images using various capturing and digitization technologies. Many approaches have been reported in the literature for the identification of wind turbines from satellite images by the research community.

2. LITERATURE REVIEW

Object classification from satellite images is very challenging in the present scenario. From, the literature Convolutional Neuronal Networks (CNN) architectures are currently seen as state-of-the-art for such problems. Several methodologies have been proposed for the identification of wind turbines and fault detection in wind turbines.

(Wang et.al, 2016) explored a framework for the identification of wind turbine gearboxes using a deep neural network with the application of a dropout algorithm during the training process to avoid overfitting. They applied the proposed framework in real-world scenarios from wind farms in China. They benchmarked the proposed framework against the gearbox monitoring based on data from oil temperature. (Xiao et.al, 2021) implemented an Attention Octave Convolution (AOCTConv) approach which has been applied to the ResNet-50 backbone network (AOC–ResNet50) for fault detection of wind turbine converters. The proposed model has been applied to 10 min SCADA system data and achieved an accuracy of 98%. (Ciaburro et.al, 2021) proposed support vector machine (SVM) for wind turbine acoustic monitoring. They applied the Boruta algorithm for feature extraction. SVM and

artificial neural networks (ANN) have been used for the detection of the operating conditions of the wind turbine. A comparative study has been carried out between the models. The accuracy achieved by the SVM model is 91.8% as compared to the ANN model. (Delgado et.al, 2021) presented LSTM-based approach to visualize and analyze wind turbine data. The proposed model has been applied to the collected data from the SCADA System. Wind features like speed, direction, generated active power, and theoretical power was predicted and a comparative study was been carried out with state-of-the-art methods. An effective approach for dynamic detection of offshore wind turbines from spaceborne synthetic aperture radar (SAR) Sentinel-1 satellite data using Random Forest (RF) technique has been proposed (Xu et.al, 2022). The pre-processing operation has been applied to reduce the speckle noise using a lee filter and ocean wave clutter was mitigated by using a constant false alarm rate (CFAR) technique. An accuracy of 93.67% has been achieved with the proposed model which has the advantages of large-scale monitoring and high precision. (Miguel-Ángel et.al, 2020) explored the capacity of different hybrid architectures of semantic segmentation models to extract wind turbines in high-resolution aerial ortho imagery. LinkNet and E_cientNet-b3 have been used as the backbone to optimize the recognition and extraction of features (wind turbines). The authors evaluated the performance of the models in five different areas of the Spanish territory and achieved a great success rate. (Han et.al. 2018) proposed the U-Net technique for identifying wind turbines quickly and precisely from high-resolution remote sensing images. To improve the accuracy of the model, the context information between wind turbines and their shadows has been learned by the U-Net network. The model has achieved an F1 score of 97%. (Xiao et.al, 2022) constructed an ensemble model for the prediction of blade icing fault in the wind turbine. A GMDH-based selective deep ensemble (GSDE) model has been introduced by combining convolution neural network (CNN) with recurrent neural network (RNN), long short-term memory (LSTM), and gated recurrent unit (GRU). A Chi-square test has been carried out for the construction of training sets in series. The proposed model has been applied to supervisory control and data acquisition (SCADA) systems and outperformed as compared to other models. (Asilpour et.al, 2020) introduced a fractional order dynamic neural network (FODNN) optimize with particle swarm optimization (PSO) for the identification of wind turbines and achieved a success rate.

Residual Network (ResNet) has been widely considered and successfully applied to numerous applications like the classification of chest X-ray images for detecting COVID-19 pneumonia (Huang et.al, 2022, Ikechukwu et.al, 2021, Showkat et. al,2022, Aswathy et.al, 2021) skin cancer diagnosis (Medhat et. al,2022), diagnosis of psoriasis (Li et.al, 2021), canopy segmentation for mechanical harvesting of apples (Zhang et.al, 2019), skin lesion analysis (Guo et.al, 201), fault diagnostic system for rolling element bearings (Grover et. al,2022), off-type identification in plants (Jaya et.al, 2022), wind turbine gearbox failure (Wang et. al,2016). From the literature, very limited work has been carried out in the direction of the identification of wind turbines from satellite imagery. On the other hand, deep neural network ResNet has been successfully applied to many applications areas for the classification of images. In this research work, a deep CNN method ResNet-50 is suggested for the identification of wind turbines from satellite imagery. There are 50 deep layers in ResNet-50 convolutional neural network. A comparative study is carried out with other ResNet architectures like ResNet-18, ResNet-34, Resnet-101, and ResNet-152 based on their performances. The finding reveals the effectiveness of ResNet-50 in resolving the above issue. This paper contains numerous sections and is organized as follows. Section II demonstrates the literature review. Section III deals with the dataset used and pre-processing approach carried out to remove all kinds of distorts present in the satellite image and proposed model. Section IV presents all experimental work carried out and empirical results obtained. Subsequently, the conclusion is articulated in Section V.

3. RESEARCH METHODOLOGY

3.1 Data Set

The dataset used in this piece of research work is built on top of the Kaggle Dataset. The dataset contains satellite images of wind turbine patches and background images in different geographical areas. The dataset contains two types of images, Images of wind turbines with background and only background without wind turbine patches. In this study, a subset of the wind turbine dataset is used for experimentation and evaluation purposes. The data consist of 500 images with wind turbine patches and 500 background images. In this study, two different partitions of the dataset are used. The first partition includes 80% of the training and 20% of the validation dataset. The second partition includes 70% of the training and 30% of the validation dataset. Figure 1 (a) Shows five samples of images with wind turbine patches and Figure 1(b) shows five samples of background images from the dataset.

Figure 1(a): Sample images containing patches of the wind turbine.

Figure 1(b): Sample background images without wind turbine.

3.2 Pre Processing

Pre Processing is an important technique in image processing used to enhance the image so that it can be interpreted in a better way. Satellite images may contain inadequate information. By pre-processing, we can enhance some required features for further phases of image processing. In this paper median filtering which is nonlinear filtering is used to remove salt and pepper noises from the satellite images with window size 3. Here the median values of neighbouring pixels are used to replace the pixel value. Figure 2(a) shows the median filter applied to five samples of wind turbine patches. Figure 2(b) shows the median filter applied to five samples of background images.

Figure 2(a): Median filter applied to wind turbine patches.

Figure 2(b): Median filter applied to background images.

3.3 Proposed Model

In this piece of research work, the proposed model is based on the residual structure ResNet50 (He, et.al, 2016) to avoid the problem of gradient disappearance and to improve the performance classification model. The research methodology Figure 3 shows the approach used in this research methodology. According to the figure, in the proposed model pre-processing is carried out in the initial stage of investigation using a median filter followed by feature extraction with ResNet architectures followed by classification which identifies wind turbines.

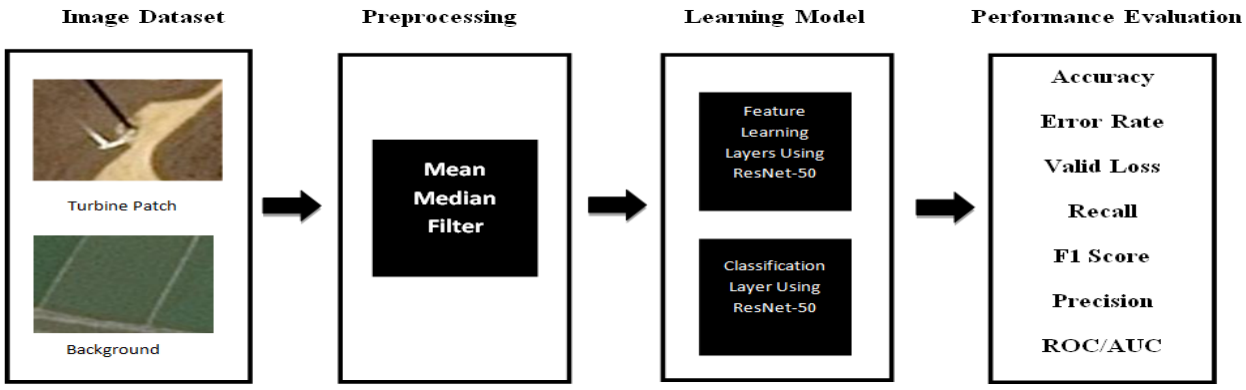

Figure 3: Research flow of the proposed model

3.4 Deep Learning Model using ResNet

A residual neural network (ResNet) is an artificial neural network (ANN).The problem of training very deep networks has been alleviated with the introduction of ResNet or residual networks. These ResNets are made up of Residual Blocks. ResNet solves the problem of the vanishing/exploding gradient by using the skip connections technique**.** The skip connection skips a few layers and connects directly to the output in the training phase (He et.al, 2016) which is shown in figure 4.

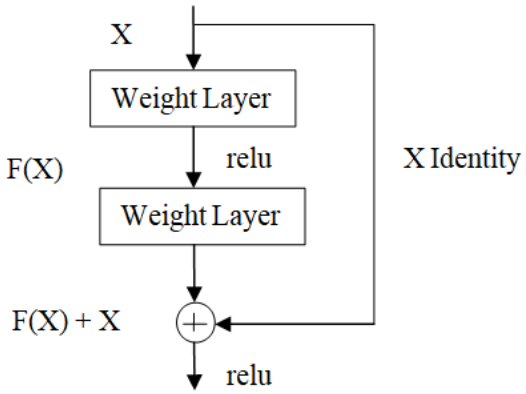

Figure 4: Residual learning: A building block

The pre-trained CNN model typically extracts features using its core architecture and learned weights. The features extracted are then introduced for classification purposes which involve optimization, architectural tuning, and parameter optimization by adding new trainable parameters to the network. Like all CNN ResNet extracts relevant features during the initial step to reduce the computational complexity for successive stages. The top convolution base layers are responsible for accomplishing this task. After features are extracted, the top layers of the convolutional base are frozen and considered untrainable, while the succeeding convolutional layers that are closer to the output features are considered trainable for improved feature extraction. The residual network (ResNet) was developed by He et. al, In 2016 [22].ResNet architecture skips connection The ResNet model's performance does not degrade when the layers of the architecture are increased, which is one of its benefits. Apart from a reduction in computational complexity, it has better training ability. It skips connections on two to three layers containing Rectified Linear Activation Unit (ReLU) and batch normalization. ResNet is most suitable for image classification than other CNN due to its ability to extract well-defined features from images. In this paper, the performance of Resnet-50 is compared with other ResNet models like ResNet-18, ResNet-34, ResNet-101, and ResNet-152. Although each ResNet design has a different number of layers, they all operate on the same premise.

The architecture of ResNet-18 and ResNet-34 contains two layers and the architecture of ResNet-50, ResNet-101, and ResNet-152 contain three layers. In the first two layers of the ResNet architecture, convolutions of size 7 × 7 and max-pooling of size 3 × 3 with stride number 2 are carried out (Showkat et. al, 2022). The input size of the

image taken is 128 × 128. The structure of different ResNet architectures (Showkat et.al, 2022) is explicated in Figure 5.

Layer name	Output size	18 Layers	34 Layers	50 Layers	101 Layers	152 Layers
Convol_1	64X64	7 X 7,64,stride=2				
Convol_2	32X32	3 X 3, Max pool, stride=2				
		$\begin{bmatrix} 3X3 & 64 \\ 3X3 & 64 \end{bmatrix} X\ 2$	$\begin{bmatrix} 3X3 & 64 \\ 3X3 & 64 \end{bmatrix} X\ 3$	$\begin{bmatrix} 1X1 & 64 \\ 3X3 & 64 \\ 1X1 & 256 \end{bmatrix} X\ 3$	$\begin{bmatrix} 1X1 & 64 \\ 3X3 & 64 \\ 1X1 & 256 \end{bmatrix} X\ 3$	$\begin{bmatrix} 1X1 & 64 \\ 3X3 & 64 \\ 1X1 & 256 \end{bmatrix} X\ 3$
Convol_3	16X16	$\begin{bmatrix} 3X3 & 128 \\ 3X3 & 128 \end{bmatrix} X\ 2$	$\begin{bmatrix} 3X3 & 128 \\ 3X3 & 128 \end{bmatrix} X\ 4$	$\begin{bmatrix} 1X1 & 128 \\ 3X3 & 128 \\ 1X1 & 512 \end{bmatrix} X\ 4$	$\begin{bmatrix} 1X1 & 128 \\ 3X3 & 128 \\ 1X1 & 512 \end{bmatrix} X\ 4$	$\begin{bmatrix} 1X1 & 128 \\ 3X3 & 128 \\ 1X1 & 512 \end{bmatrix} X\ 8$
Convol_4	8 X 8	$\begin{bmatrix} 3X3 & 256 \\ 3X3 & 256 \end{bmatrix} X\ 2$	$\begin{bmatrix} 3X3 & 256 \\ 3X3 & 256 \end{bmatrix} X\ 6$	$\begin{bmatrix} 1X1 & 256 \\ 3X3 & 256 \\ 1X1 & 1024 \end{bmatrix} X\ 6$	$\begin{bmatrix} 1X1 & 256 \\ 3X3 & 256 \\ 1X1 & 1024 \end{bmatrix} X\ 23$	$\begin{bmatrix} 1X1 & 256 \\ 3X3 & 256 \\ 1X1 & 1024 \end{bmatrix} X\ 36$
Convol_5	4 X 4	$\begin{bmatrix} 3X3 & 512 \\ 3X3 & 512 \end{bmatrix} X\ 2$	$\begin{bmatrix} 3X3 & 512 \\ 3X3 & 512 \end{bmatrix} X\ 3$	$\begin{bmatrix} 1X1 & 512 \\ 3X3 & 512 \\ 1X1 & 2048 \end{bmatrix} X\ 3$	$\begin{bmatrix} 1X1 & 128 \\ 3X3 & 128 \\ 1X1 & 2048 \end{bmatrix} X\ 3$	$\begin{bmatrix} 1X1 & 512 \\ 3X3 & 512 \\ 1X1 & 2048 \end{bmatrix} X\ 3$
	1 X 1	Average Pooling 1000, Softmax function				

Figure 5: The architecture of different ResNet models

4. Experimental Results

This section covers the training details and experimental results carried out. This section reports the results of several ResNet models on various metrics. All of the ResNet models—ResNet18, ResNet34, ResNet50, ResNet101, and ResNet152—are trained independently on the same dataset before performance comparison. During training, all models are trained with the same fixed training parameters.

The dataset is portioned into two parts, the training and validation set. The models were trained to distinguish between wind turbine patches and background images without wind turbine patches. Every model undergoes cross-entropy (CE) loss function during training, while the Adam algorithm executes training-stage optimization. A batch size of 16 is used to train the models. The initial learning rate employed in this study is 0.01 and there is 100 epochs in total. After numerous simulations, the final results have been recorded. The proposed model is assessed on two varieties of validation data. 80% of the training data and 20% of the validation data are included in the first partition. The second partition includes 70 % of training and 30% of validation data. In the initial stage of the pre-processing operation is carried out using a median filter. Learning of features by the model is done by the convolution layer. The model was developed with Python (Open Source). The evaluation measures are computed by taking average values ten times.

4.1 Performance Measurement

The metrics used for performance evaluation of the proposed model include accuracy, training loss, validation loss, error rate, specificity, sensitivity, Receiver Operating Characteristics-Area under the curve (ROC-AUC) curve, and F1 score. Further, the result obtained is compared with other ResNet architectures like ResNet-18, ResNet-34, ResNet-101, and ResNet-152. The above evaluation metrics are defined with the terms correctly identified wind turbine patches (True Positives, TP), Correctly identified background images(True Negative, TN), incorrectly identified wind turbine patches (False Negative, FN), and incorrectly identified background images(False Positive, FP). Figure 6 (a) shows the training and validation loss of all models with 80% training and 20% validation dataset for 100 epochs. Figure 6(b) shows the training and validation loss of all models with 70% training and 30% validation dataset for 100 epochs.

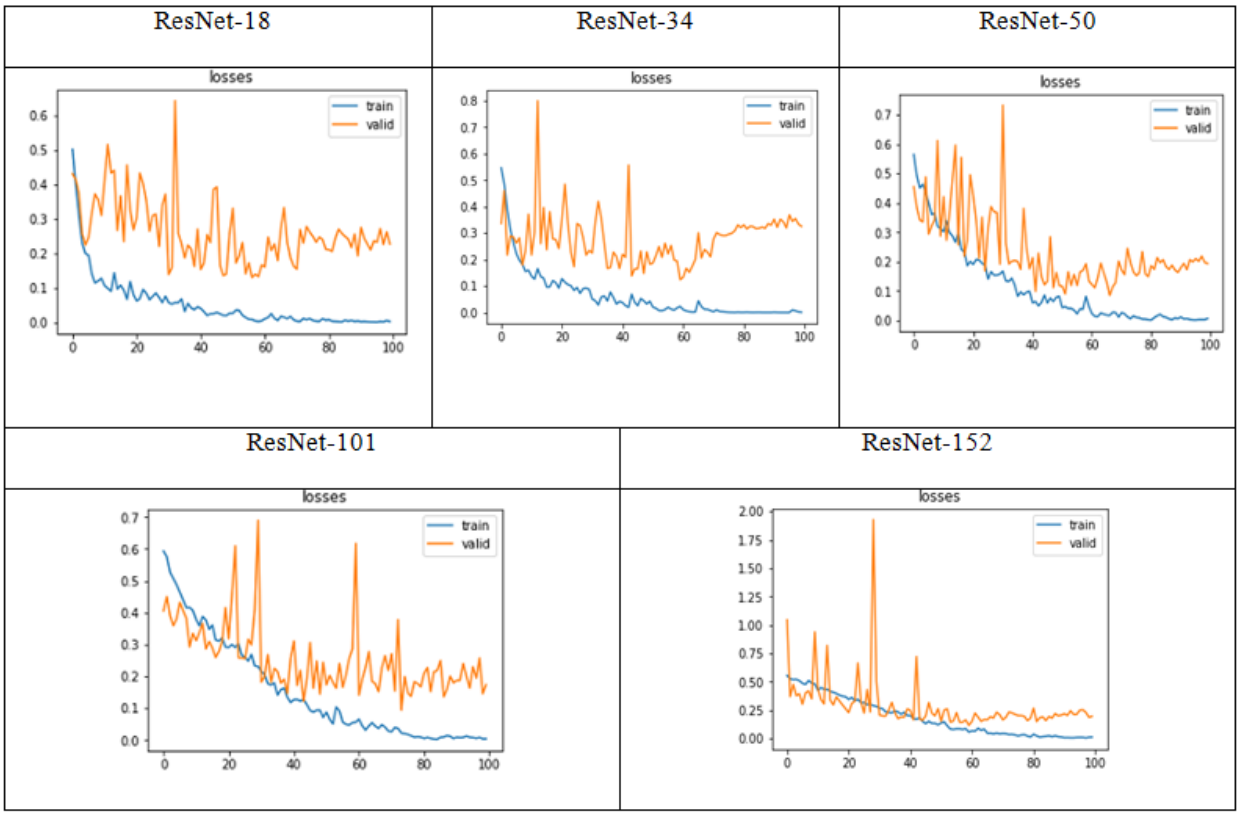

Figure 6 (a): Training and validation loss of all models with 80% of training and 20% of validation dataset

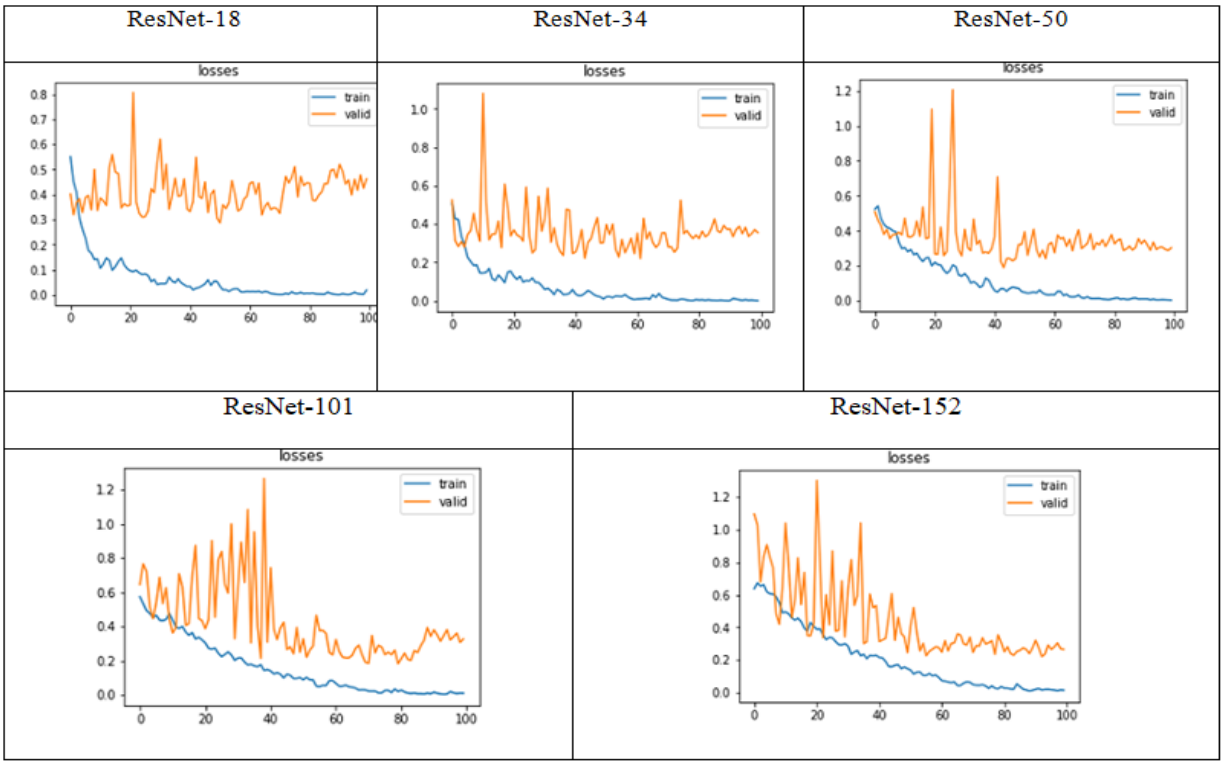

Figure 6 (b): Training and validation loss of all models with 70% of training and 30% of validation dataset

4.2 Confusion Matrix

The confusion matrix provides a foundation for the evaluation of metrics. There are two classes in the dataset. 0 refers to the background and is denoted as negative. 1 refers to wind turbine patches, and is denoted as positive cases. In the dataset, there are 500 negative cases and 500 positive cases. The class distribution is highly balanced. The confusion matrix obtained from the experimental result using the proposed model is shown in figures 7(a) and figure 7(b). Figure 7(a) shows the confusion matrix of all models for 80% of the training dataset and 20% of the validation dataset. Figure 7(b) shows the confusion matrix of all models for 70% of the training dataset and 30% of the validation dataset.

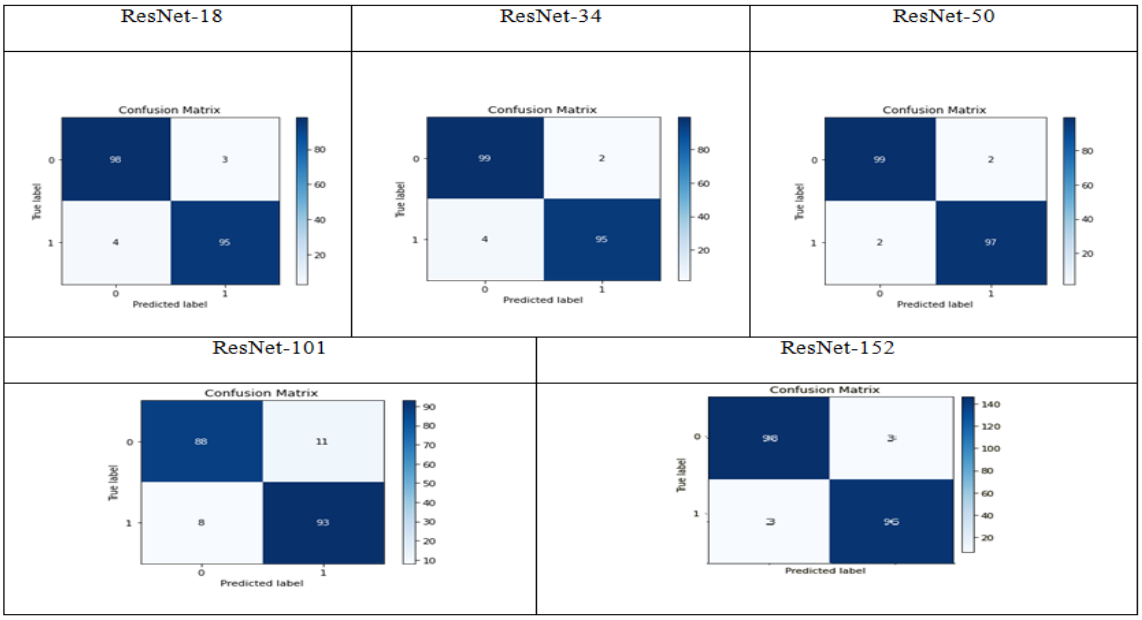

Figure 7(a): Confusion matrix of different models with 80% of the training and 20% of the validation dataset

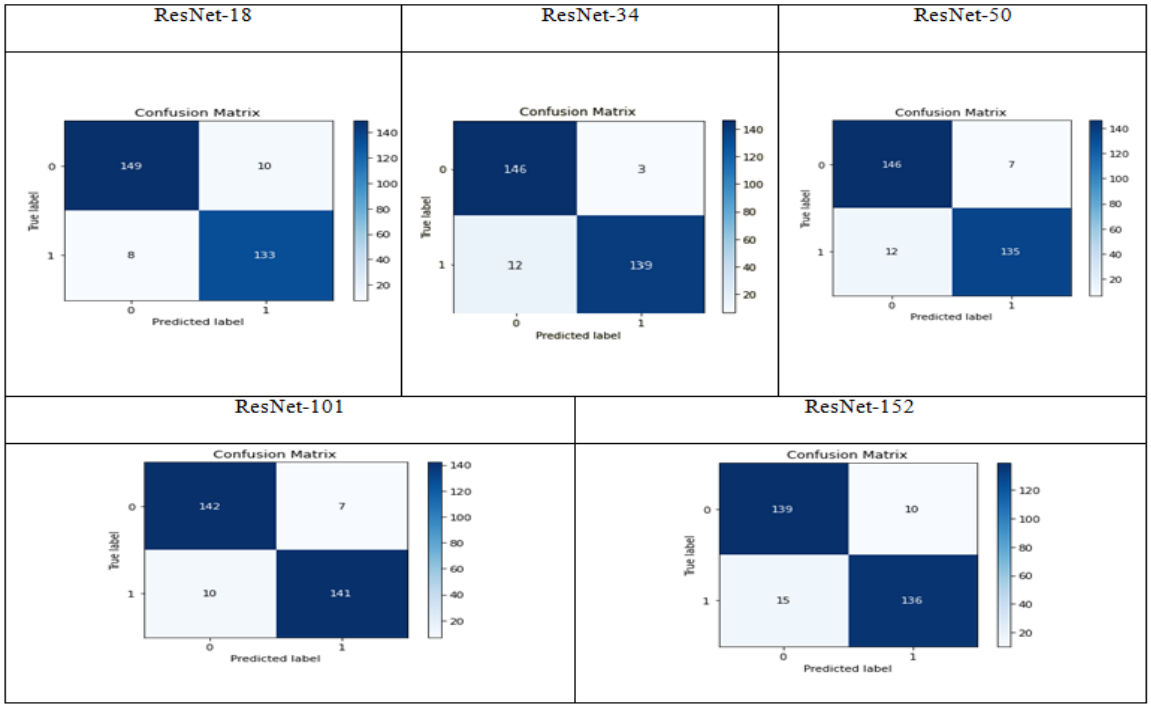

Figure 7(b): Confusion matrix of different models with 70% of the training and 30% of the validation dataset

4.3 Accuracy

When the dataset is highly balanced, accuracy is the most used metric for evaluating the model performance. Accuracy shows how accurately a model is performing. Mathematically, it is defined as the ratio of the sum of all correctly classified classes to the total number of cases under evaluation. The accuracy value of 1 is considered the best value and 0 is considered the worst value. The confusion matrix can be used to compute accuracy as follows.

$$Accuarcy = (TP + TN)/(TP + TN + FP + FN) \quad (1)$$

The plot of the accuracy of different models is shown in figure 8(a) with 80% of the training dataset and 20% of the validation dataset. Figure 8(b) shows the plot of the accuracy of different models for 70% of the training dataset and 30% of the validation dataset.

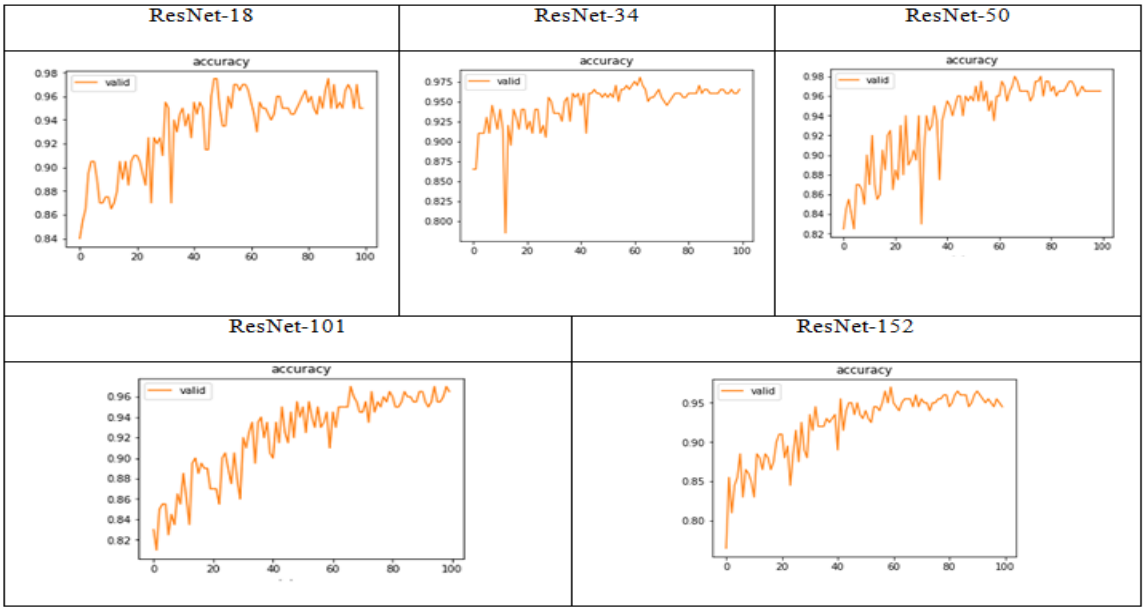

Figure 8 (a): Accuracy of different models with 80% of training and 20% of validation dataset.

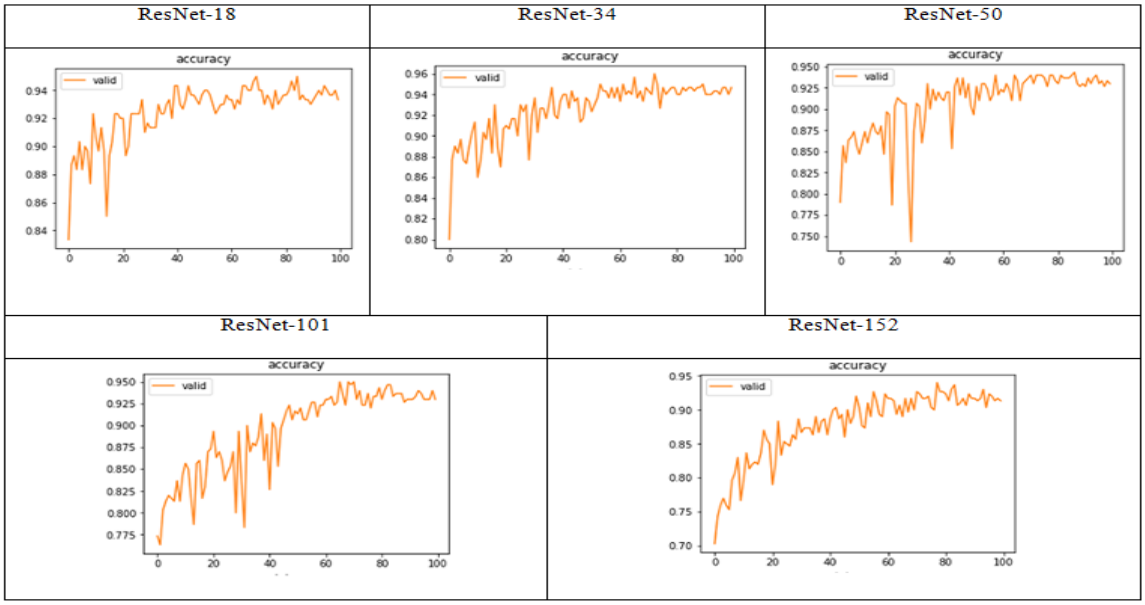

Figure 8(b): Accuracy of different models with 70% of training and 30% of validation dataset

4.4 Sensitivity/True Positive Rate

Sensitivity measures how correctly a model classifies positive values. It measures how sensitive a model is. Mathematically, it is the ratio of True Positives to Actual Positives. Sensitivity is defined as the ratio of positive cases (TP) that are correctly classified as the sum of true positives (TP) and false negatives (FN). It is also called true positive rate (TPR). The mathematical formula for the calculation of sensitivity is as follows

$$Sentitivity = (TP)/(TP + FN) \quad (2)$$

Sensitivity or the recall score of different ResNet models with 80% of the training and 20% of the validation dataset is shown in figure 9(a). The Recall score of different ResNet models with 70% of the training and 30% of the validation dataset is shown in figure 9(b).

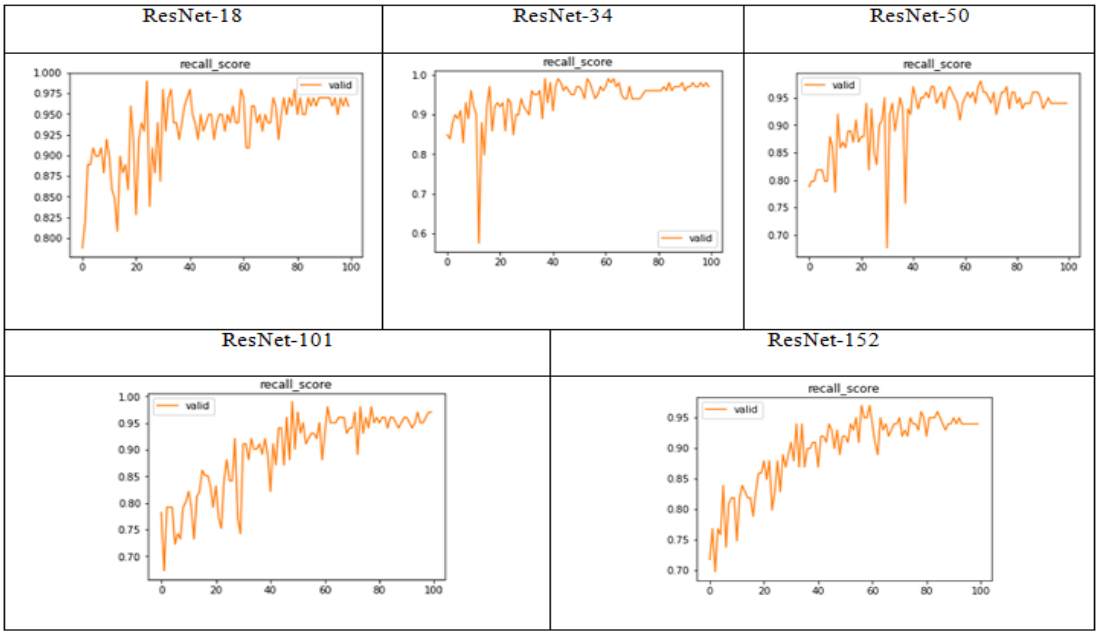

Figure 9 (a): Recall score of different ResNet models with 80% of the training and 20% of the validation dataset

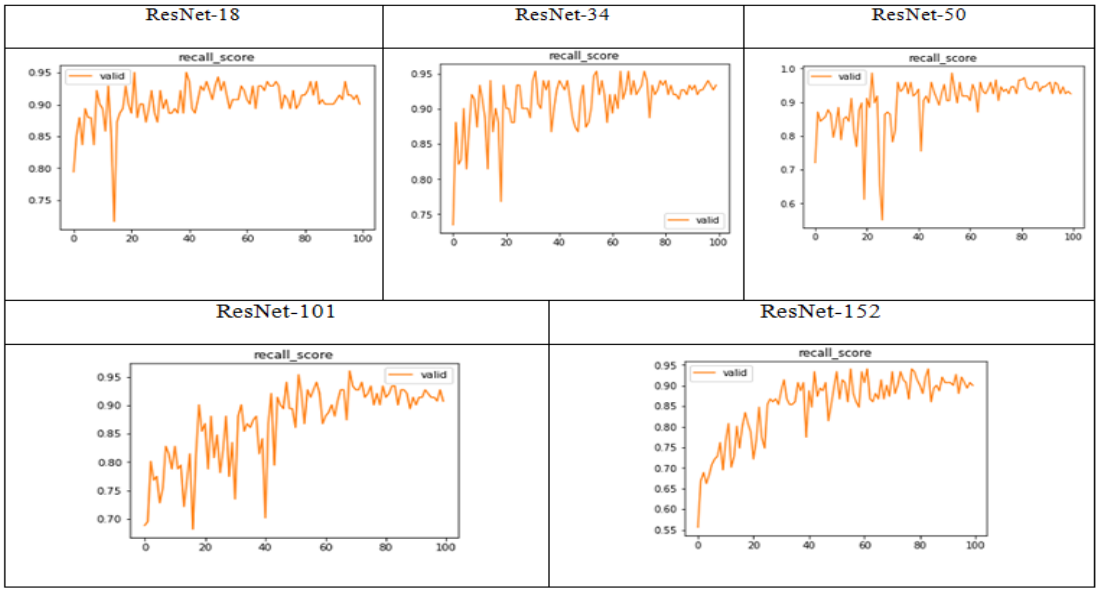

Figure 9 (b): Recall score of different ResNet models with 70% of the training and 30% of the validation dataset

4.5 Specificity/ true negative rate and precision

Specificity measures how correctly a model classifies Negative cases. It measures how specific a model is. Mathematically, it is the ratio of true negatives to actual negatives. Specificity is defined as the ratio of negative cases (TN) that are correctly classified as the sum of true negatives (TN) and false positives (FP). It is also called True Negative Rate (TNR). The mathematical formula for the calculation of sensitivity is as follows

$$Specificity = (TN)/(TN + FP) \quad (3)$$

The mathematical formula for the calculation of precision is as follows

$$Precision = (TP)/(TP + FP) \quad (4)$$

The precision score of different ResNet models with 80% of the training and 20% of the validation dataset is shown in figure 10(a). The precision score of different ResNet models with 70% of the training and 30% of the validation dataset is shown in figure 10(b).

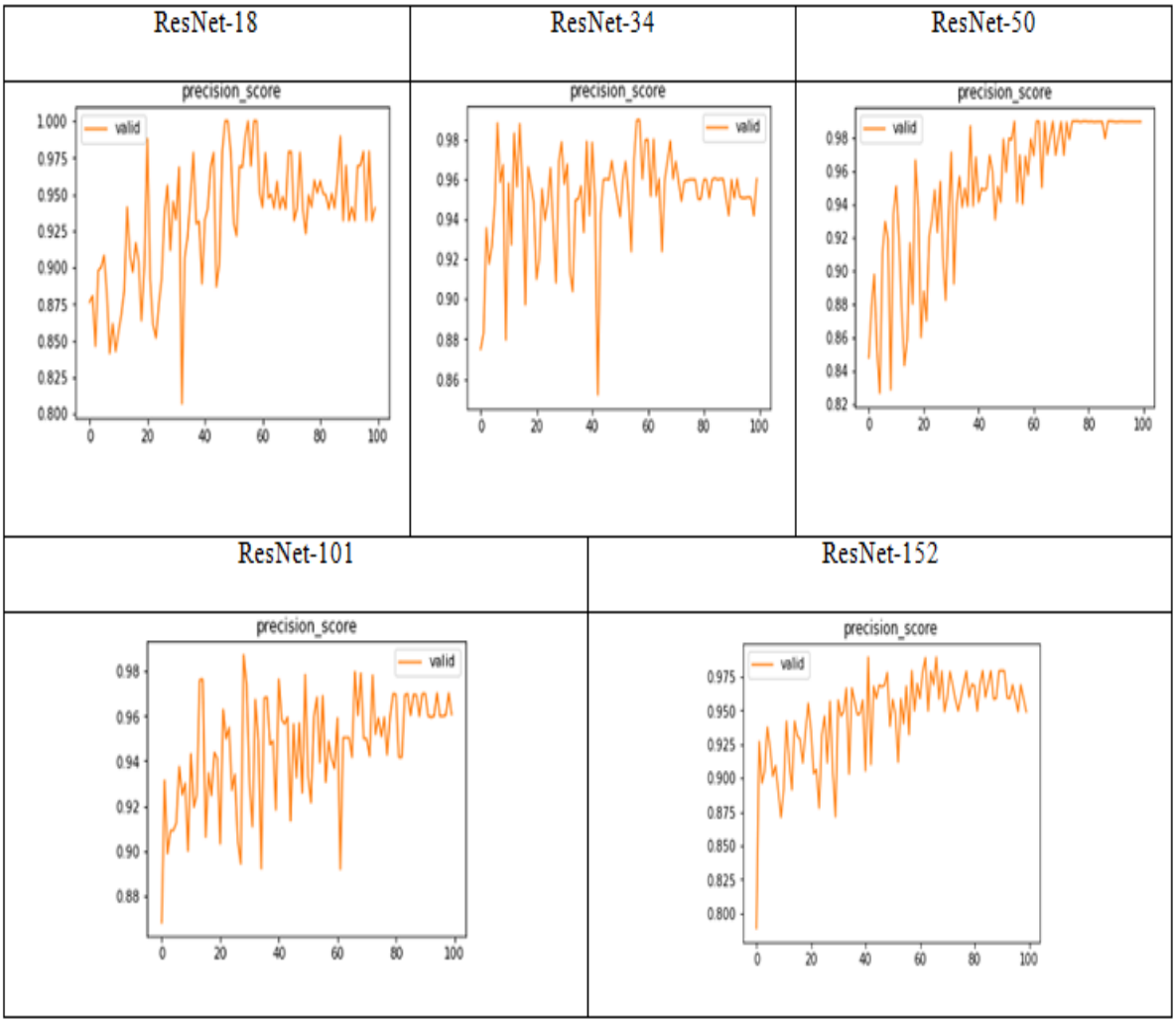

Figure 10 (a): Precision score of different ResNet models with 80% of the training and 20% of the validation dataset

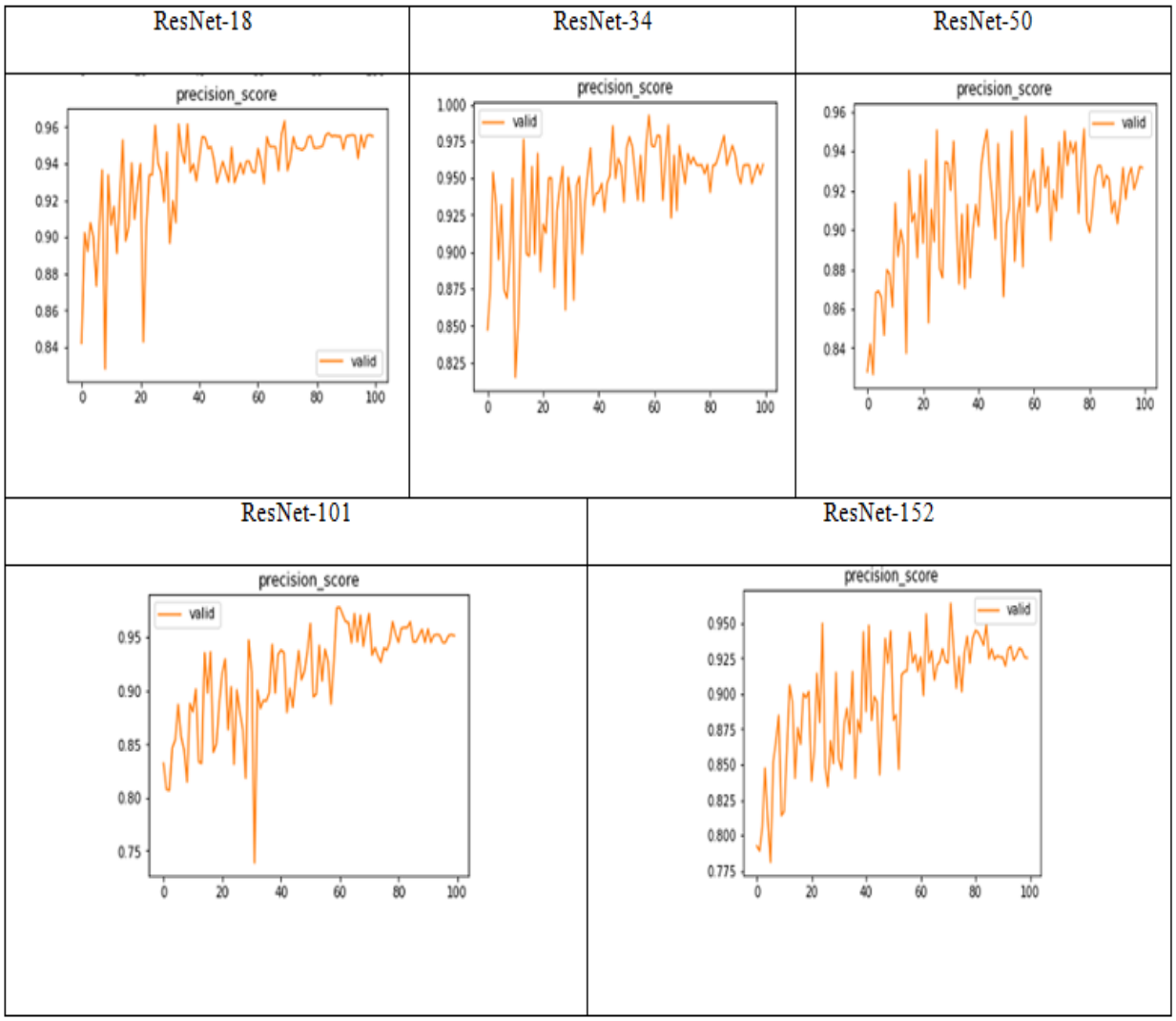

Figure 10 (b): Precision score of different ResNet models with 70% of the training and 30% of the validation dataset

4.6 F1 Score

The F1-score is the corresponding class's weighted average of recall and precision. The lowest value is 0, while 1 is the highest. Following are the calculations

F1 Score = (2*Precision*Recall) / (Precision + Recall)

Figure 11(a) shows F1 score of different models with 80% of the training and 20% of the validation dataset. Figure 11(b) shows F1 score of different models with 70% of the training and 30% of the validation dataset.

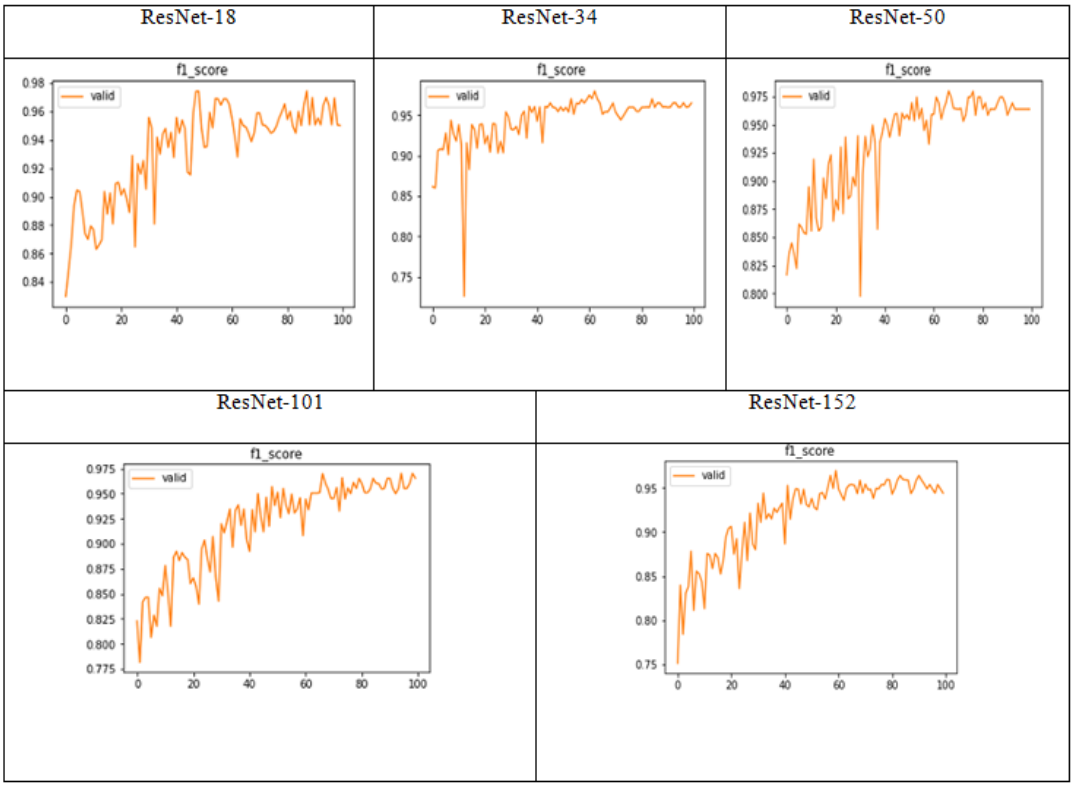

Figure 11 (a): F1 score of different ResNet models with 80% of training and 20% of validation dataset

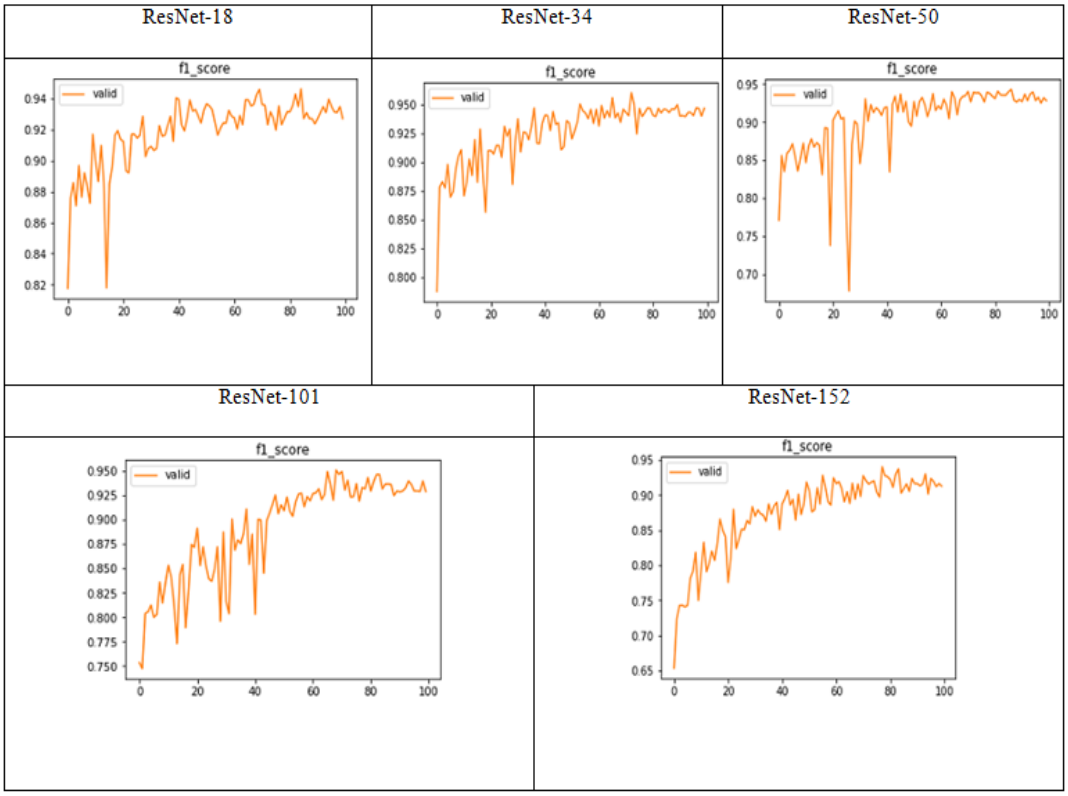

Figure 11 (b): F1 score of different ResNet models with 70% of training and 30% of validation dataset

4.7 Receiver Operating Characteristic (ROC) curve

Receiver operating characteristics (ROC) is a visualization chart. To assess the effectiveness of the classification model, ROC uses the area under the curve (AUC) metric. Receiver operating characteristic curve (ROC) and area under curve (AUC) are related terms. The x-axis in ROC is utilised to represent the false positive rate, and the y-axis represents the true positive rate. In this curve, a threshold value is used for classification. In this proposed model predicted output above the threshold value is considered as belonging to label 1 and below the threshold value is considered as belonging to label 0. The bottom reference of a classification is represented with AUC of 0.5. AUC value with 1 is considered as the best value and AUC with value is considered worst value. Figure 12(a) shows the ROC curve of each class for different models with 80% of training and 20% of validation dataset. Figure 12(b) shows the ROC curve of each class for different models with 70% of training and 30% of validation dataset.

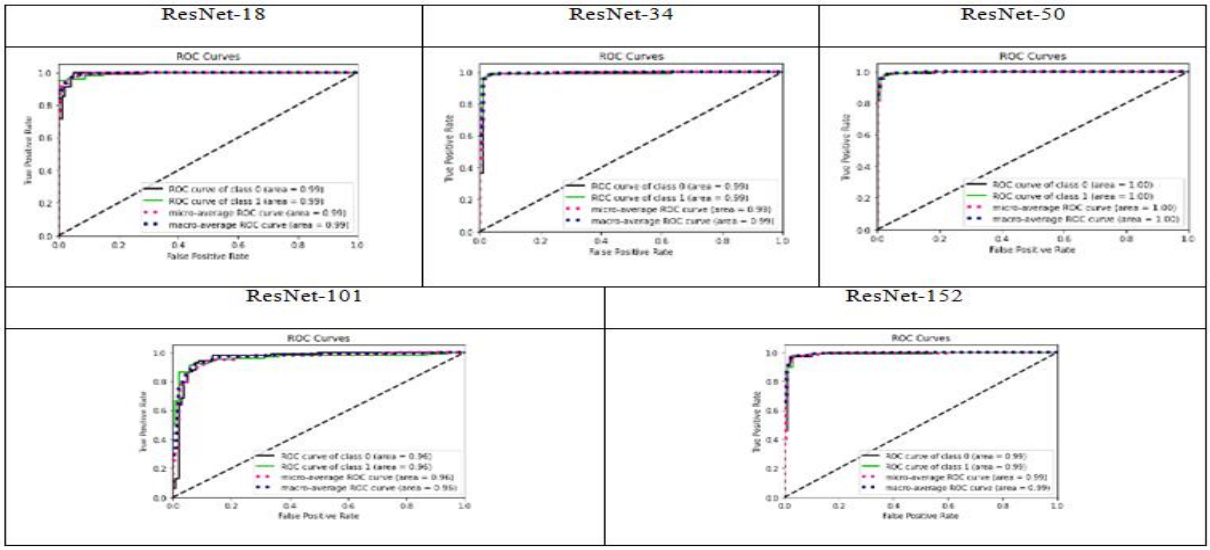

Figure 12(a): ROC curve of different models with 80% of the training and 20% of the validation dataset.

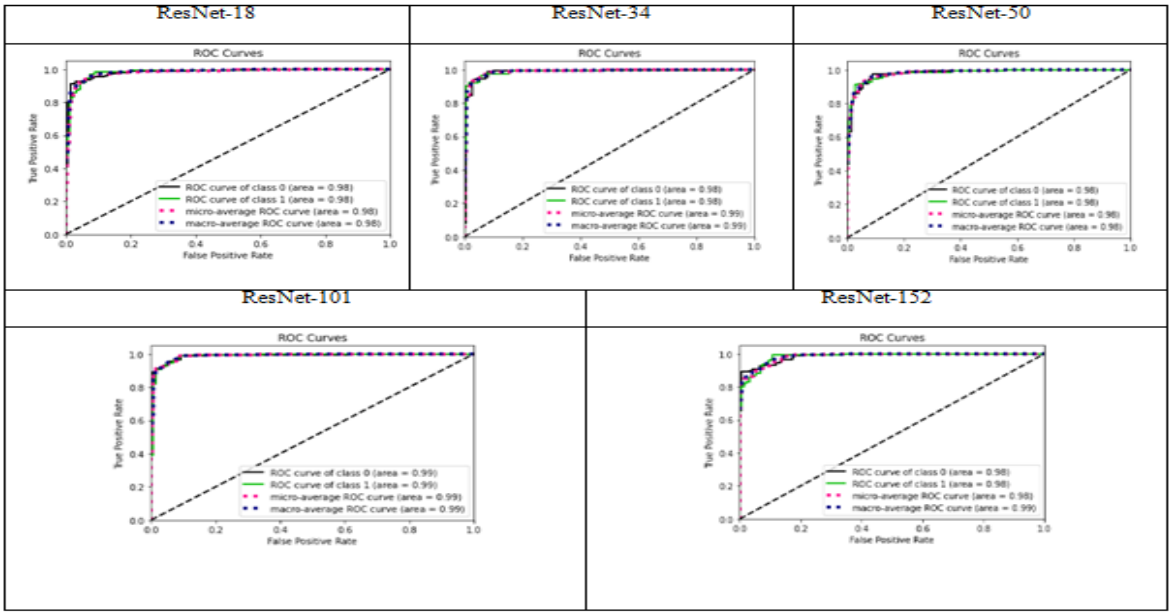

Figure 12(b): ROC curves of different models with 70% of the training and 30% of the validation dataset.

From the experimental study, the highest accuracy obtained with models Resnet-18, Resnet-34, Resnet-50, and Resnet-152 is 96.50%, 97%,98%,90.5%, and 97% respectively with 80% of training and 20% of validation dataset. Resnet-101 has achieved 94.33 % of accuracy with 70% of training and 30% of the validation dataset which is shown in Tables 1 and 2. Fig. 6(a) shows the best validation performance at epoch 67 for ResNet-50 with 80% of t---raining and 20% validation dataset. From the experimental result, the proposed model outperformed as compared to other models with an accuracy of 98% on the validation dataset. When compared to other models, the ResNet-50 offers the most consistent performance in terms of accuracy, sensitivity, and specificity values, according to the empirical findings.

Table 1: Performance comparison of all ResNet architecture under different metrics with 80% training and 20% of validation dataset.

Model	Accuracy	Valid Loss	Recall	F1 Score	Precision	Roc
Resnet-18	96.50	0.129722	95.95	96.44	96.93	99.34
Resnet-34	97.00	0.123733	95.95	96.93	97.93	99.01
ResNet-50	98.00	0.192542	97.97	97.97	97.97	99.64
Resnet-101	90.50	0.212400	98.01	96.58	95.19	97.36
Resnet-152	97.00	0.220517	90.06	91.58	93.15	98.46

Table 2: Performance comparison of all ResNet architecture under different metrics with 70% training and 30% of validation dataset.

Model	Accuracy	Valid Loss	Recall	F1 Score	Precision	Roc
Resnet-18	94.00	0.070337	97.97	97.00	96.03	99.77
Resnet-34	95.00	0.193330	94.03	96.27	98.61	99.05
Resnet-50	93.66	0.188284	91.83	93.42	95.07	97.96
Resnet-101	94.33	0.243339	92.05	92.66	93.28	97.33
Resnet-152	91.66	0.110056	96.77	96.46	96.15	99.43

5. CONCLUSION

In this present work, a framework of ResNet-50 architecture is introduced for the identification of wind turbines from satellite imagery, which has proved to be feasible in experiments. The proposed model is also compared with other ResNet architecture like ResNet-18, ResNet-34, ResNet-101 and, ResNet-152. From experimental results, ResNet-50 provided the highest accuracy of 98% as compared to other models which is a highly superlative result as compared to other models and earlier works in the field. Experimental result shows that a deeper residual network does not necessarily provide a better result than other networks. Instead, this can be achieved with 50 layers of ResNet architecture. The proposed model is found to be more suitable. It is observed that (Han et.al, 2018) gave an accuracy of 97% which is lesser than our model. According to the experimental study carried out, the suggested model may generalise unknown dataset, which is a promising development for creating a reliable computer-aided wind turbine identification system using satellite images.

REFERENCES

Aslipour Z., Yazdizadeh A., (2020), Identification of Wind Turbine using Fractional Order Dynamic Neural Network and Optimization Algorithm, International Journal of Engineering, 33(2), 277-284, https://dx.doi.org/10.5829/ije.2020.33.02b.12.

Aswathy A.L., Anand Hareendran S., Vinod Chandra S., (2021), COVID-19 diagnosis and severity detection from CT-images using transfer learning and back propagation neural network, Journal of Infection and Public Health, 14, 1435-1445. https://doi.org/10.1016/j.jiph.2021.07.015

Ciaburro G., Iannace G., Puyana-Romero V., Trematerra M., (2021), Machine Learning-Based Tools for Wind Turbine Acoustic Monitoring, Appl. Sci. 11, 6488, https://doi.org/10.3390/app11146488.

Delgado I., Fahim M., (2021), Wind Turbine Data Analysis and LSTM-Based Prediction in SCADA System, Energies, 14, 125, https://dx.doi.org/10.3390/en14010125.

Grover C., Turk N., (2022). A novel fault diagnostic system for rolling element bearings using deep transfer learning on bispectrum contour maps, Engineering Science and Technology, an International Journal, 31, 1-6, https://doi.org/10.1016/j.jestch.2021.08.006.

Guo S., Yang Z. (2018) Multi-Channel-ResNet, An integration framework towards skin lesion analysis, Informatics in Medicine Unlocked, 12, 67-74, https://doi.org/10.1016/j.imu.2018.06.006.

Han, M., Wang, H., Wang, G., Liu, Y., (2018), Targets mask U-Net for Wind Turbines Detection in Remote Sensing Images, The International Archives of the Photogrammetry, Remote Sensing and Spatial Information Sciences, Volume XLII-3, https://doi.org/10.5194/isprs-archives-XLII-3-475-2018.

He, K., Zhang, X., Ren, S. & Sun, J. (2016) Deep residual learning for image recognition. in Proceedings of the IEEE Conference on Computer Vision and Pattern Recognition ,770–778, https://doi.org/10.1109/CVPR.2016.90.

Huang, Q., Lei, Y., Xing, W., He, C., Wei, G., Miao, Z., Hao, Y., Li, G., Wang, Y., Li, Q., Li, X., Li, W. & Chen, J. (2022), Evaluation of Pulmonary Edema using Ultrasound Imaging in Patients with Covid-19 Pneumonia Based on A Non-Local Channel Attention ResNet, Published by Elsevier Inc.,48, 945-953, https://doi.org/10.1016/j.ultrasmedbio.2022.01.023.

Ikechukwu A.V., Murali S., Deepu R., Shivamurthy, R.C., (2021), ResNet-50 vs. VGG-19 vs. training from scratch: A comparative analysis of the segmentation and classification of Pneumonia from chest X-ray images, Global Transitions Proceedings, 2, 375-381, https://doi.org/10.1016/j.gltp.2021.08.027

Brindha G.J., Gopi, E.S. (2022), Masking technique based attention mechanism for off-type identification in plants, Machine Learning with Applications, Published by Elsevier Ltd, 8, 1-6, https://doi.org/10.1016/j.mlwa.2022.

LI, P., YI, Na., Changsong, D., Sheng, L. & Hui, M. (2021) Research on classification diagnosis model of psoriasis based on deep residual network, Digital Chinese Medicine, 4(2), 92-101, https://doi.org/10.1016/j.dcmed.2021.06.003.

Callejo M.A.M, Cira C.I., Alcarria R., Justel J.J.A., (2020), Optimizing the Recognition and Feature Extraction of Wind Turbines through Hybrid Semantic Segmentation Architectures, 12, 1-16, http://dx.doi.org/10.3390/rs12223743

Medhat S., Galil H.A., Aboutabl, A.E., Saleh H. (2022), Skin cancer diagnosis using convolutional neural networks for smartphone images: A comparative study, Journal of Radiation Research and Applied Sciences, 15, 262-267. https://doi.org/10.1016/j.jrras.2022.03.008.

Showkat S., Qureshi, S., (2022), Efficacy of Transfer Learning-based ResNet models in Chest X-ray image classification for detecting COVID-19 Pneumonia, Chemometrics and Intelligent Laboratory Systems, 224, 1-10, https://doi.org/10.1016/j.chemolab.2022.104534.

Wang, L., Long, H, Xu, J., Liu, R., (2016), Wind Turbine Gearbox Failure Identification with Deep Neural Networks, IEEE Transactions on Industrial Informatics, DOI 10.1109/TII.2016.2607179.

Xiao C., Liu Z., Zhang T., Zhang X., (2021), Deep Learning Method for Fault Detection of Wind Turbine Converter, Appl. Sci., 11, 1280, https://doi.org/10.3390/app11031280

Xiao J., Li, C., Liu, B., Huang J., Xie, L., (2022), Prediction of wind turbine blade icing fault based on selective deep ensemble model, Knowledge-Based Systems,242, 2022,108290. https://doi.org/10.1016/j.knosys.2022.108290.

Xu, Z., Zhang, H., Wang, Y., Wang, X., Xue, S. & Liu, W. (2022) Dynamic detection of offshore wind turbines by spatial machine learning from spaceborne synthetic aperture radar imagery, Journal of King Saud University – Computer and Information Sciences, 34(5), 1674-1686, https://doi.org/10.1016/j.jksuci.2022.02.027.

Zhang X., Fu L., Karkee M., Whiting M.D., Zhang Q. (2019) Canopy Segmentation Using ResNet for Mechanical Harvesting of Apples, IFAC PapersOnLine 52-30, 300–305.